Available online at www.sciencedirect.com

SciVerse ScienceDirect

Ceramics International 38 (2012) 6235–6241

CERAMICS INTERNATIONAL

www.elsevier.com/locate/ceramint

The effect of nano-Cr_2O_3 on solid-solution assisted sintering of MgO refractories

H.R. Zargar*, C. Oprea, G. Oprea, T. Troczynski

Materials Engineering Department, University of British Columbia, Vancouver, BC, Canada, V6T 1Z4

Received 11 April 2012; received in revised form 27 April 2012; accepted 27 April 2012
Available online 17 May 2012

Abstract

The effect of Cr_2O_3 particle size on the densification of magnesia refractories was investigated. Magnesia grains (< 45 μm) were mixed with 2 wt% of micro-Cr_2O_3 (2 μm) and nano-Cr_2O_3 particles (10–20 nm) and sintered at 850–1450 °C, for 5 h in air. The progress of the densification and phase evolution of samples was studied with the support of X-ray diffraction phase analysis (XRD), Fourier transformer infrared spectroscopy (FTIR) and scanning electron microscopy (SEM). It was shown that the densification of magnesia was enhanced by reducing the particle size of the added chromia to the range of 20 nm. According to the phase analysis results, the higher dissolution rate of Cr_2O_3 in MgO in the MgO–Cr_2O_3 system was responsible for the faster densification of nano-Cr_2O_3 containing mixes.

Keywords: A. Sintering; Magnesia refractories; Nano-Cr_2O_3; Solid-solution

1. Introduction

MgO refractories are good candidates for the lining of cement and steel furnaces, owing to the high melting temperature of MgO (2800 °C) and to the fact that it is inert toward the basic slags. However, they have poor thermal shock resistance and high thermal conductivity, which limited their applications. Several researchers addressed these shortcomings by including different additives, such as SiO_2, Al_2O_3, Cr_2O_3, TiO_2, ZrO_2, $MgCl_2$, and WO_3 [1–10]. Chaudhuri et al. [11] studied the effect of ZrO_2 and TiO_2 on magnesia and showed that both oxides enhanced its densification. The TiO_2 reacted with the calcia in magnesia, forming calcium titanate, while ZrO_2 was dissolved in MgO. Han et al. [12] found that the addition of WO_3 to MgO resulted in the formation of phases with low melting points ($MgWO_4$ and $CaWO_4$) in the magnesia grain boundaries; the presence of liquid phases resulted in a higher densification. In fact, the formation of $CaWO_4$ during sintering led to a decrease in the CaO/SiO_2 ratio in MgO and as such, to reduced amounts of $3CaO \cdot SiO_2$ (C_3S) and $2CaO \cdot SiO_2$ (C_2S) phases.

In recent years, nano-crystalline ceramics and the application of nanoparticles to improve the ceramic processing have attracted considerable interest, as the mechanical, optical, electrical, and magnetic properties are crystallite-size sensitive. Zhao et al. [13] studied the addition of nano-Fe_2O_3 (average particle size of 17 nm) into the matrix of magnesia–chrome ceramics and reported that the sintering temperature was reduced by about 150 °C. Also, adding up to 2 wt% nano-Fe_2O_3 progressively increased the compressive and bending strength at every sintering temperature [13]. Azhari et al. [14] found that adding iron oxide with an average particle size of 60 nm enhanced the formation of magnesioferrite spinel at much lower temperatures (1350 °C, compared to 1550 °C for samples without nano-Fe_2O_3). Adding an identical amount of micron-sized Fe_2O_3 ($d < 45$ μm) led to the formations of less $MgFe_2O_4$ spinel, with lower compressive and bending strength than the samples containing nano-Fe_2O_3. The deterioration of the mechanical properties was attributed to the higher degree of the homogeneity of $MgFe_2O_4$ in the microstructure of samples containing nano-Fe_2O_3,

*Corresponding author. Tel.: +1 60 4822 3122.
E-mail address: ms4he@interchange.ubc.ca (H.R. Zargar).

0272-8842/$36.00
http://dx.doi.org/10.1016/j.ceramint.2012.04.077

compared to the micron-sized Fe_2O_3 samples. The dilatometry results showed that the onset sintering temperature (when the shrinkage started) was ~1100 °C for the samples with 4 wt% nano-Fe_2O_3, ~50 °C lower than for the reference sample (with no nano-Fe_2O). The lower sintering temperature of the samples containing nano-Fe_2O_3 was attributed to the decrease in dihedral angle between the magnesia grains [14].

Similar effects of nanoparticles—reducing the sintering temperature and improving the mechanical properties—were also reported for non-oxide ceramics. Wang et al. [15] coated Si_3N_4 particles with Al_2O_3 and Y_2O_3 via the citrate nitrate sol–gel procedure, and showed that the nano-sized oxides formed in-situ on the Si_3N_4 grains acted as sintering aids, reducing the sintering temperature to 1250 °C, compared to 1480 °C for the samples without additives. The reduction of sintering temperature by the nanoparticles was attributed to the crystallization of YAG phase at a very low temperature (600 °C); the YAG phase reacted with the SiO_2 on the Si_3N_4, resulting in the early formation of the liquid phase. Consequently, the liquid phase existed over a wider temperature range and for a more prolonged duration. Braulio et al. [16] studied the effect of nano-Al_2O_3 and nano-MgO on the expansion behavior of alumina–magnesia refractory castables. The mixture of the nano-oxides (nano-AM) was proposed as a novel additive that could accommodate the expansion caused by the spinel formation and enhance the sinterability of alumina–magnesia castables. The increased densification of nano-AM was measured based on the spinel expansion temperature in the expansion-temperature diagrams [16]. However, there was a 3 wt% limit in the addition of nano-Al_2O_3, above which no distinguishable changes in the sintering properties were measured. Qiu et al. [17] investigated the densification of AlN powders in the presence of nano-AlN; substituting 2 wt% of AlN with nano-AlN increased the density from 2.78 to 3.28 (g/cm^3) after firing at 1600 °C. Due to its higher activity and surface area, the nano-AlN acted as a sintering additive, increasing the green density and facilitating the mass transport.

To the best of our knowledge, there are few published results on the effect of the nano-additives formed in-situ on the sintering temperature of ceramic materials. Most existing sources [13–19] are limited to the application of pre-formed nanoparticles. In the present work, the effect of the nano-Cr_2O_3 formed in-situ on the sintering of magnesia grains was investigated. The nano-chromia precursor was coated on the MgO grains and the densification of the mixes containing nano-Cr_2O_3 was compared to that of the samples containing micro-Cr_2O_3. This methodology also ensured the uniform distribution of the chromia additive on the magnesia grains.

2. Experimental procedures

Two sets of samples containing magnesia with 2 wt% nano-Cr_2O_3, and magnesia with 2 wt% micro-Cr_2O_3 were prepared. The citrate nitrate sol–gel process was used to prepare the samples containing the nano-Cr_2O_3. The precursors used were chromium nitrate nonahydrate (Fisher UN2720), citric acid (Aldrich 11328BO) as chelating agent and ammonium hydroxide (Fisher Scientific Canada 321275) to adjust the pH. The citric acid suppresses the precipitation during the pH change and acts as a "fuel", reacting with nitrates to generate heat and facilitate the Cr_2O_3 formation [19,20]. The resulting Cr_2O_3 particles were 10–20 nm in size, as seen in the TEM image in Fig. 1. In order to coat the magnesia grains with the synthesized nano-Cr_2O_3, the magnesia grains (MagChem P98, <45 μm) were immersed into the as-prepared 0.1 M chromia sol, ensuring that the amount of nano-Cr_2O_3 in MgO–Cr_2O_3 was 2 wt%. The chromia sol was subsequently aged for 2 h at 80 °C in order to gel it. The mixture was then dried for 24 h at 100 °C and calcined at 650 °C for 2 h, to minimize the amount of volatile species and to form nano-Cr_2O_3 particles on the MgO grains. In order to prepare the samples with micro-Cr_2O_3, the magnesia grains were mixed with 2 wt% micro-chromia (Fisher C.I. 77288, $d_{50}=2$ μm) in a ball mill. In both cases the coated grains were mixed with 5 wt% poly-vinyl alcohol (PVA) solution and pressed uniaxially into pellets under 80 MPa pressure. The specimens were heated with a constant heating rate (5 °C/min) in air, up to the sintering temperatures (850–1450 °C) and soaked for 5 h. The Fourier transform infrared spectroscopy (FTIR) tests were conducted with a Perkin Elmer Spectrum 100 instrument (USA) in transmission mode and KBr as a diluting agent. The phase analysis was performed with a Rigaku Multiflex X-ray diffractometer (Japan), using the Cu-Kα radiation. The microstructure analysis was performed using a Hitachi S3000N (Japan) scanning electron microscope, equipped with an electron dispersive X-Ray spectroscopy (EDS) detector and Quartz X-One X-ray post-processing software. The TEM was performed using a Hitachi H-800

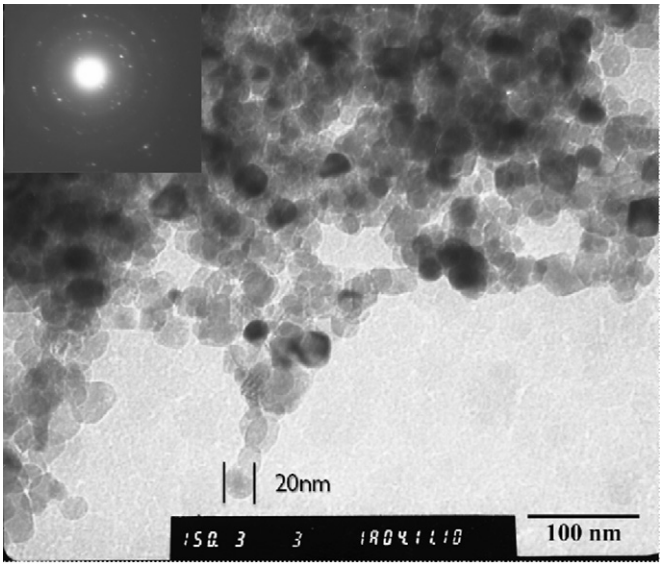

Fig. 1. TEM image of synthesized nano-Cr_2O_3.

transmission electron microscope. The thermal analysis of samples was performed with a Linseis (Germany) differential thermal analyzer.

3. Results and discussion

Fig. 2 shows the DTA patterns of the samples with both nano and micro-Cr_2O_3. In both cases, relatively sharp exothermic peaks were seen between 200 °C and 470 °C. The exothermic peaks of the ammonium nitrate dissociation were only seen in the samples with nano-Cr_2O_3, at 347 and 387 °C. For both sets of samples, a peak at 460 °C was present, and it was attributed to the PVA combustion [21]. However, the peak at 460 °C might also result from the burnout of the residual carbon. In addition, two broad exothermic peaks were observed at about 600 °C and 1000 °C in the specimens with nano-Cr_2O_3, while there was only one broad peak at ~1000 °C in the specimens with micro-Cr_2O_3. Fig. 3 shows the XRD patterns of samples with nano and micro-Cr_2O_3 sintered at temperatures lower than 1000 °C. The XRD peaks of $MgCr_2O_4$ were first observed for the specimen with nano-Cr_2O_3 fired at 850 °C, indicating that the crystallization of $MgCr_2O_4$ started around that temperature [22]. However, for the samples with micro-Cr_2O_3, the $MgCr_2O_4$ spinel was first observed only at 950 °C. Based on this, we propose that the higher reactivity of the nano-Cr_2O_3 effected the spinel formation at lower temperatures than in the samples with micro-Cr_2O_3. At temperatures below 850 °C, the spinel formation via the counter-diffusion of magnesia and chromia was initiated by the expected high reactivity of nano-Cr_2O_3 precursors. Because the XRD technique could not identify the spinel formation below 850 °C, FTIR was performed on the samples fired at 650 °C and on pure MgO, Cr_2O_3 and $MgCr_2O_4$, in order to analyze the reaction at that temperature. In the FTIR patterns shown in Fig. 4, the broad –OH band centered on 3400 cm^{-1} and the H_2O vibration band centered at 1650 cm^{-1}. The peak around 2800 cm^{-1} is related to the stretching of the C–H vibrations from the organic compounds (citrates) used during synthesis [19]. In the sample calcined at 650 °C (Fig. 4A) the C–H groups are still present, but they disappeared in the calcined powders at higher temperatures (1450 °C), and the band at 600 cm^{-1}, corresponding to the metal–oxygen–metal bond (M–O–M), became sharper and stronger [23]. Since the latter peak was also observed in the FTIR pattern of $MgCr_2O_4$, the broad peaks at 650 and 1000 °C indicates the $MgCr_2O_4$ formation. Comparing the XRD and FTIR patterns, it is proposed that the spinel formation in the samples containing nano-Cr_2O_3 occurred in two steps, the first one as low as 650 °C, due to the high reactivity of the nano-Cr_2O_3. In contrast, only one peak at about 1000 °C was observed in the samples with micro-Cr_2O_3. This confirms that the nano-Cr_2O_3 precursors reacted with the MgO grains (substrate) and formed $MgCr_2O_4$ in the 600–750 °C temperature range. Since the temperature was relatively low, it is expected that the formed $MgCr_2O_4$ had a structure with defects and low crystallinity [22], thus no XRD peaks for $MgCr_2O_4$ were observed at temperatures below 850 °C.

Fig. 5 shows the nano-morphology of $MgCr_2O_4$ particles formed on the MgO grains in samples calcined at 850 °C. According to the EDS analysis, the bright phase was composed of 31.6 wt% MgO and 68.4 wt% Cr_2O_3,

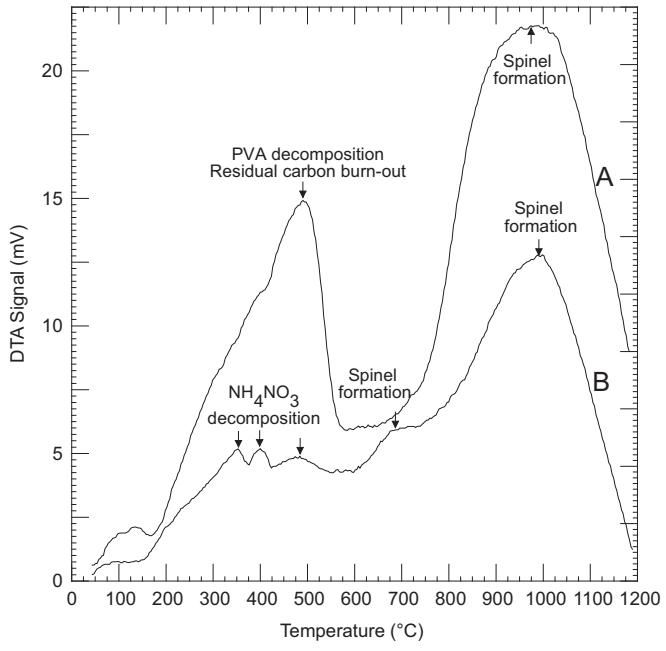

Fig. 2. DTA spectra of specimens containing 2 wt% (A) micro-Cr_2O_3, (B) nano-Cr_2O_3.

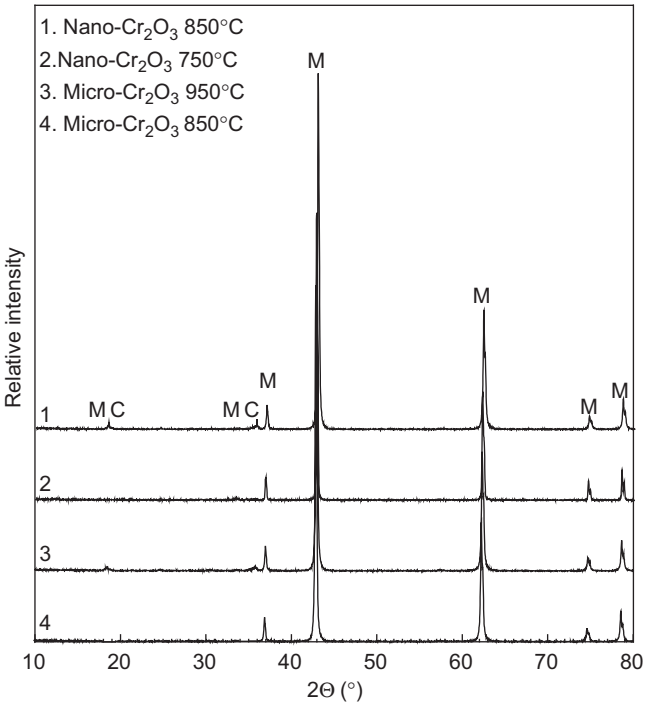

Fig. 3. XRD patterns of MgO-2 wt% nano- and micro-Cr_2O_3 samples sintered at 750–950 °C for 5 h; M: MgO, MC: $MgCr_2O_4$ spinel.

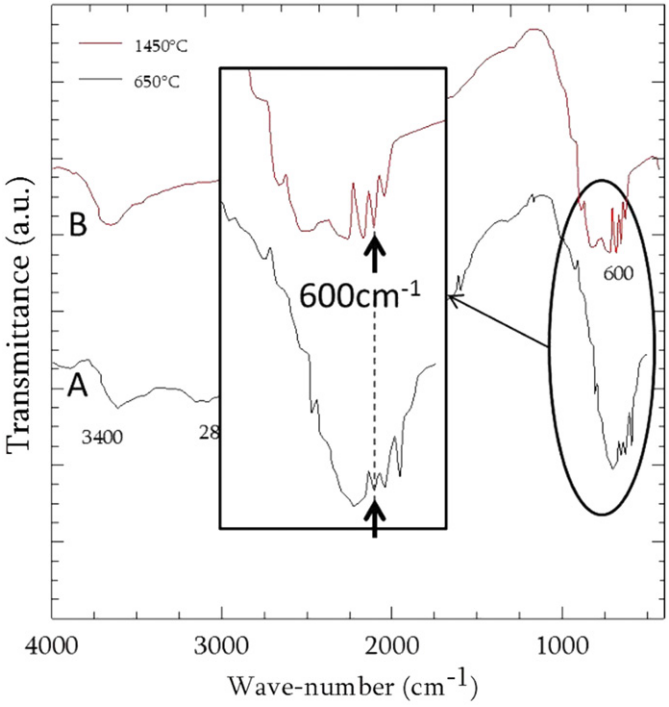

Fig. 4. FTIR spectra of samples containing nano-particles calcined at (A) 650 °C and (B) 1450 °C.

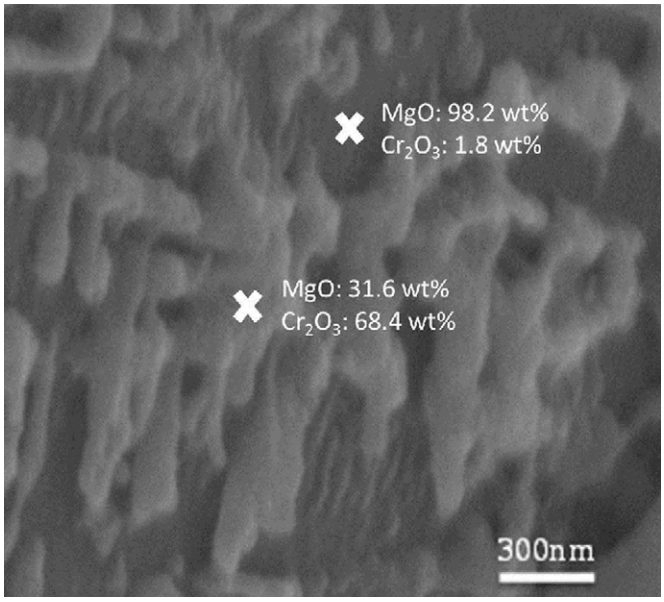

Fig. 5. BSE microstructure of 2 wt% nano-Cr_2O_3 coated magnesia grains calcined at 850 °C, showing the formation of $MgCr_2O_4$ spinel on the magnesia grains.

which is somewhat different from the stoichiometric composition (21 wt% MgO and 79 wt% Cr_2O_3) of spinel in the XRD patterns. This was attributed to the small particle size of the $MgCr_2O_4$ formed on the MgO substrate, which caused the detection of additional Mg from the surrounding MgO.

Increasing the heat treatment temperature resulted in the instability of $MgCr_2O_4$, due to the solid-solution formation, as predicted by the MgO–Cr_2O_3 phase diagram [24]. As a result, the $MgCr_2O_4$ peaks were not observed in the samples air-quenched from the sintering temperature; instead, a shift of up to 0.24° 2θ was observed in the MgO peaks location (Fig. 6), which indicated the formation of the solid-solution. Based on these results, the lattice parameter was determined in both sets of samples, in order to compare the extent of solid-solution formation as a function of the heat treatment temperature. The incident XRD beam was Cu-Kα1, and the (111) peak of MgO was analyzed on 0.15 ± 0.01 g of pulverized (< 45 μm) sintered samples, with a X-ray time per step of 2 s and 2θ step of 0.02° for a 2θ range of 10–80°. In order to calculate the error of measurement, titanium of 99.99% purity was selected as the internal standard sample. Based on the *d*-spacing displacement of the titanium peaks, the combined standard uncertainty was calculated at 0.0015 Å.

Fig. 7 shows the variation of the lattice parameter versus the sintering temperature for samples containing nano and micro-Cr_2O_3 air-quenched from the sintering temperature. The lattice parameter of all these samples decreased with increased sintering temperature. Since Cr^{+3} has smaller cationic radii (123 pm) than Mg^{+2} (144 pm), the dissolution resulted in the reduction in the lattice parameter and the displacement of MgO peaks to higher angles. The lattice parameter in the samples containing nano-Cr_2O_3 was smaller than in the samples with micro-Cr_2O_3 between 850 and 1250 °C, but had about the same value (4.162 Å) at 1350–1450 °C. This behavior can be attributed to the higher rate of the solid-solution formation in the low temperature range, due to the higher activity of the chromia nano-particles compared to the micro-particles. At higher temperatures (1350–1450 °C), the same rate of solid-solution formation was expected for both nano and micro-Cr_2O_3, owing to the grain growth and to the fact that Cr_2O_3 in both cases was in the form of a solid-solution.

The contribution of the solid-solution formation to the densification behavior of MgO samples is shown in Fig. 8. As seen, the density of the samples with nano-Cr_2O_3 increased with 12%, while for the samples with micro-Cr_2O_3 increased with only 4.8%, when sintered in the range of 850–1450 °C. It is worth noting that for the samples with micro-Cr_2O_3 no densification was observed up to 850 °C, in contrast to about 2% densification in the nano-Cr_2O_3 samples. Considering the higher increasing rate of the theoretical densities (ΔTD) for the samples with nano compared to the samples with micro-Cr_2O_3 in the sintering temperature range, the better densification of the samples containing nano-chromia was attributed to the faster solid-solution formation, hence to the enhanced atomic mobility at the sintering temperature.

The high degree of homogeneity of the nanoparticles, as well as their high reactivity due to the increased surface area, resulted in enhanced solid-solution formation, as shown by the lattice parameter change plotted in Fig. 7. As previously reported by Kolar et al. [25] on the sintering of

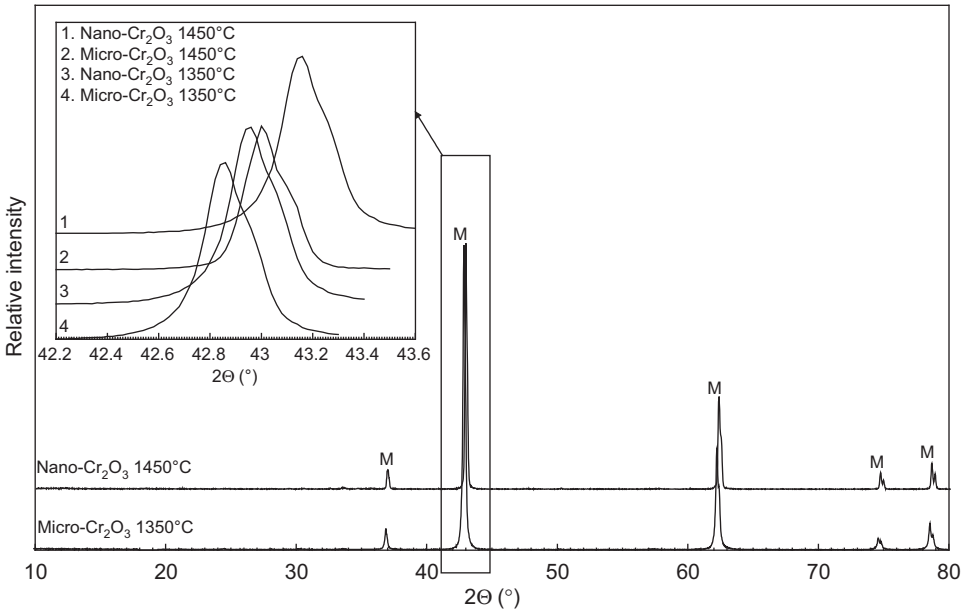

Fig. 6. XRD patterns of MgO-2 wt% nano and micro-Cr_2O_3 samples sintered at 1450 °C for 5 h; M: MgO.

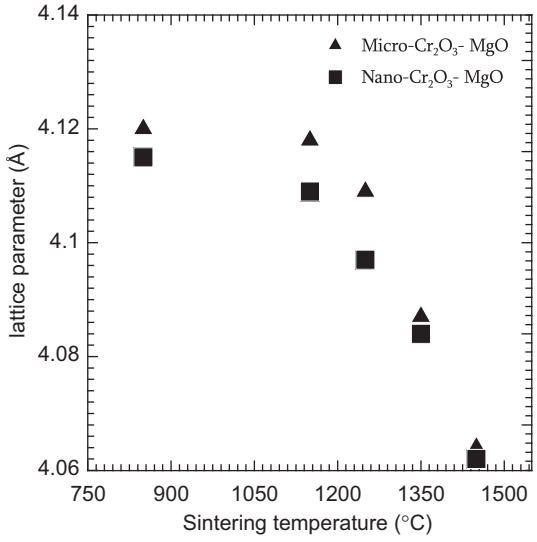

Fig. 7. Variation of lattice parameter for MgO samples containing nano and micro-Cr_2O_3 after sintering at various temperatures.

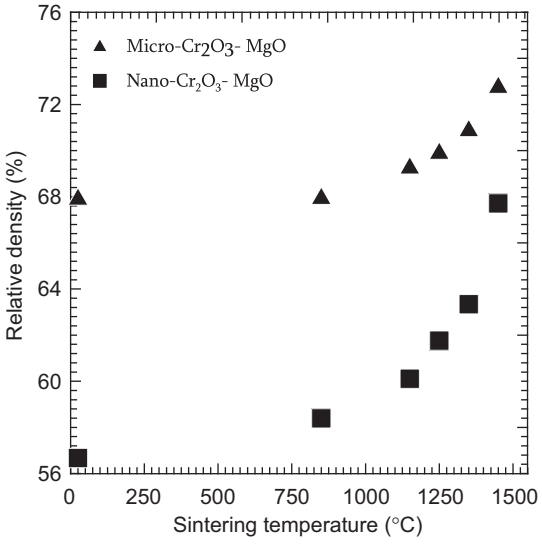

Fig. 8. Variation of the density of MgO-2 wt% nano and micro-Cr_2O_3 samples sintered at 750–1450 °C for 5 h.

$BaTiO_3$–$SrTiO_3$ solid-solutions, one-directional diffusion of species increased the ''Kirkendall effect'', which changed the structure of the neck area by creating voids, and thus decreased the extent of densification. For more than 5 wt% $BaTiO_3$ in $SrTiO_3$ (or vice versa), the degree of sintering decreased due to the heterogeneous solid-solution formation. Comparing our results with those reported by Kolar, we propose that the atomic mobility, hence the densification, were increased due to the homogeneous distribution of the nano-Cr_2O_3, and to the vacancies formation, as for every $2Cr^{+3}$ that diffused to the MgO/Cr_2O_3 interface, $3Mg^{+2}$ must also diffuse there [26,27]. Since in the ionic materials the vacancies are responsible for the diffusion mechanisms, the increased number of vacancies could enhance the diffusion rate and thus result in higher densification rates. Moreover, the enhanced atomic mobility lasts over a wider temperature range, compared to the samples containing micro-Cr_2O_3; this might be a reason for the better densification of MgO with nano-Cr_2O_3. In fact, for the samples with micro-Cr_2O_3, the reduced contact area between Cr_2O_3 and MgO grains led to the decreased solid-solubility of Cr_2O_3 in MgO and lowered the concentration of vacancies, compared to that of specimens with nano-Cr_2O_3.

The back scattered (BSE) SEM images of the samples air-quenched from 1450 °C are shown in Fig. 9. The

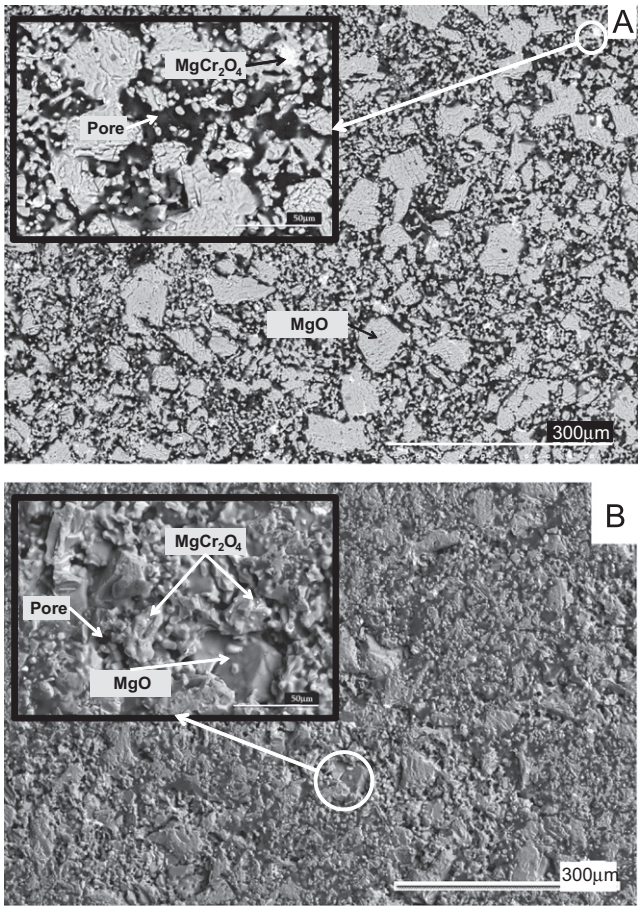

Fig. 9. BSE images of MgO-2 wt% Cr_2O_3, sintered at 1450 °C for 5 h and air-quenched (1450–1000 °C in 5 min): (A) micro- Cr_2O_3 and (B) nano-Cr_2O_3; inset show higher magnifications of the marked areas.

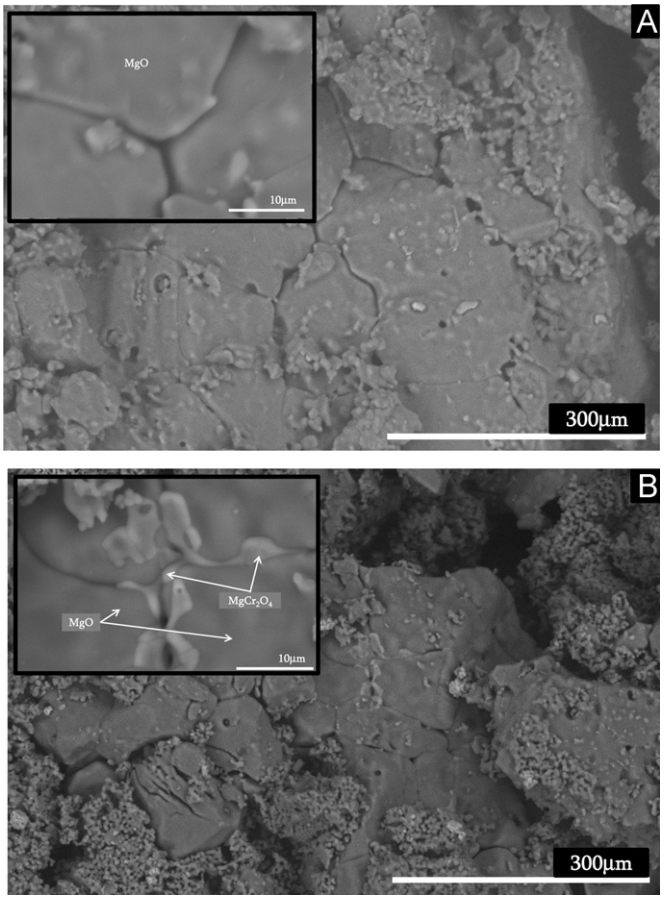

Fig. 10. BSE images of samples sintered at 1450 °C for 5 h and furnace-cooled (1450–1000 °C in 150 min): (A) MgO-2 wt% micro Cr_2O_3, and (B) MgO-2 wt% nano Cr_2O_3.

microstructure of the MgO with micro-Cr_2O_3 consists of sharp-edged magnesia grains and agglomerates of $MgCr_2O_4$ spinel, while the microstructure of the MgO with nano-Cr_2O_3 is composed of round-edged grains, indicating the solid-solution formation. Very fine $MgCr_2O_4$ spinel precipitates were observed in the microstructure of the samples containing nano-Cr_2O_3, which verifies the better solid-solubility of the samples containing nano- in comparison to micro-Cr_2O_3. The microstructure of the furnace-cooled samples is presented in Fig. 10. Due to the decrease in solid-solubility at low temperatures, a layer of $MgCr_2O_4$ precipitated at the grain boundaries of the MgO grains in the sample with nano-Cr_2O_3, while no spinel was observed in the grain boundaries of MgO grains with an identical amount of micro-Cr_2O_3. Regarding the microstructure of the samples with nano-Cr_2O_3, Layden and McQuarrie [28] reported that a certain amount of additive could enhance the densification of MgO; this quantity was close to the solubility limit of the additive in MgO. Based on his investigations, this quantity was 0.1 wt% for Cr_2O_3, and the addition of more than 0.1 wt% resulted in the precipitation of $MgCr_2O_4$ and reduced the final density of magnesia. It should be mentioned that no $MgCr_2O_4$ spinel was observed in the microstructure of the air-quenched samples, due to the higher solubility of Cr_2O_3 in MgO at 1450 °C.

4. Conclusions

We have demonstrated that the in-situ formation of chromia nano-particles is a reliable method to homogeneously introduce nano-particles into the micron-sized MgO ceramics. The Cr_2O_3 with particle size in the nano range (10–20 nm) increased the dissolution of the Cr_2O_3 into MgO at relatively low temperatures (as low as 850 °C), and consequently enhanced the densification of MgO, compared to MgO with micro-Cr_2O_3. These results indicate the effectiveness of the nano-Cr_2O_3 particles as sintering additives for MgO refractories, where the porosity is required to be below 10–15%.

Acknowledgment

The authors thank the industrial sponsors of the research consortium on refractories for non-ferrous industries at UBCeram of UBC, and the Natural Sciences and Engineering Research Council of Canada for the financial support of this project.

References

[1] G.K. Layden, M.C. Mcouarrie, Effect of minor additions on sintering of MgO, Journal of the American Ceramic Society 42 (1959) 89–92.

[2] T. Lucion, P.H. Duvigneaud, A. Laudet, J.F. Stenger, E. Gueguen, Effect of TiO_2 additions on the densification of MgO and MgO–CaO mixtures, Key Engineering Materials 264–268 (2004) 209–212.

[3] N. Petric, B. Petric, V. Martinac, N. Bogdanic, M. Mirosevic-Anzulovic, M Labor, Sintering of magnesium oxide obtained from sea water, Journal of the European Ceramic Society 13 (1994) 545–549.

[4] T. Matsumoto, A. Kato, Effects of additives on sintering of CVD-MgO powders, Ceramics International 16 (1990) 325–331.

[5] K. Hamano, Z. Nakagawa, H. Watanabe, Effect of magnesium chloride on sintering of magnesium oxide, Journal of the American Ceramic Society 10 (1984) 610–618.

[6] V. Martinac, M Labor, N. Petric, Effect of TiO_2, SiO_2 and Al_2O_3 on properties of sintered magnesium oxide from sea water, Materials Chemistry and Physics 46 (1996) 23–30.

[7] B. Zhang, Z. Wang, S. Zhang, X. Wang, Z. Xu, Effects of rare earth oxides on microstructures and properties of magnesia refractories, Key Engineering Materials 368-372 (Part 2) (2008) 1158–1160.

[8] Z. Wang, Z. Xu, B. Zhang, X. Wang, Effect of mixture of rare earth oxides on microstructure and properties of magnesia refractory, Xiyou Jinshu Cailiao Yu Gongcheng, Rare Metal Materials and Engineering 36 (2007) 373–375.

[9] J.W. Nelson, I.B. Cutler, Effect of oxide additions on sintering of magnesia, Journal of the American Ceramic Society 41 (1958) 406–409.

[10] N. Petric, B. Petric, M. Mirosevic-Anzulovic, N. Bogdanic, investigating the magnesium oxide sintering process, CFI Ceramic Forum International 65 (1988) 7–10.

[11] M. Chaudhuri, G. Banerjee, A. Kumar, S.L. Sarkar, Secondary phases in natural magnesite sintered with addition of titania, ilmenite and zirconia, Journal of Materials Science 34 (1999) 5821–5825.

[12] B. Han, Y. Li, C. Guo, N. Li, F. Chen, Sintering of MgO-based refractories with added WO_3, Ceramics International 33 (2007) 1563–1567.

[13] H. Zhao, S. Hu, H. Wang, The influence of nano-Fe_2O_3 on sintering and mechanical performance of magnesite–chrome refractory, in: Proceedings of the Unified International Technical Conference on Refractories, Osaka, Japan, 2003 pp. 284–287.

[14] A. Azhari, F. Golestani-Fard, H. Sarpoolaky, Effect of nano iron oxide as an additive on phase and microstructural evolution of Mag–Chrome refractory matrix, Journal of the European Ceramic Society 29 (2009) 2679–2684.

[15] L. Wang, W.M. Sigmund, S. Roy, F. Aldinger, Improved densification by nano-sized sintering aids for Si_3N_4, Journal of Materials Research 14 (1999) 4562–4569.

[16] M.A.L. Braulio, G.G. Morbioli, L.R.M. Bittencourt, V.C. Pandolfelli, Novel features of nanoscaled particles addition to alumina–magnesia refractory castables, Journal of the American Ceramic Society 93 (2010) 2606–2610.

[17] J. Qiu, Y. Hotta, K. Watari, K. Mitsuishi, Enhancement of densification and thermal conductivity in AlN ceramics by addition of nano-sized particles, Journal of the American Ceramic Society 89 (2006) 377–380.

[18] X. Wang, P. Xiao, Characterisation of clay sintering process using impedance spectroscopy, Journal of the European Ceramic Society 22 (2002) 471–478.

[19] A. Saberi, F. Golestani-Fard, M. Willert-Porada, Z. Negahdari, C. Liebscher, B. Gossler, A novel approach to synthesis of nanosize $MgAl_2O_4$ spinel powder through sol–gel citrate technique and subsequent heat treatment, Ceramics International 35 (2009) 933–937.

[20] K.A. Singh, L.C. Pathak, S.K. Roy, Effect of citric acid on the synthesis of nano-crystalline yttria stabilized zirconia powders by nitrate–citrate process, Ceramics International 33 (2007) 1463–1468.

[21] A.V. Tolkachev, T.V. Druzhinina, L.A. Nazar'ina, Thermal properties of polyvinyl-alcohol fibres in presence of phosphorus-containing catalyst, Khimicheskie Volokna (1997) 23–27.

[22] D. Kim, S. Oh, Agglomeration behavior of chromia nanoparticles prepared by amorphous complex method using chelating effect of citric acid, Materials Letters 59 (2005) 976–980.

[23] K. Vivekanandan, S. Selvasekarapandian, P. Kolandaivel, Raman and FT-IR studies of $Pb4(NO_3)_2(PO_4)_2$ and middot$2H_2O$ crystal, Materials Chemistry and Physics 39 (1995) 284–289.

[24] A.M. Alper, R.N. McNally, R.C. Doman, F.G. Keihn, Phase equilibria in system $MgO–MgCr_2O_4$, Journal of the American Ceramic Society 47 (1964) 30–33.

[25] D. Kolar, M. Ttrontelj, Z. Stadler, Influence of Interdiffusion on Solid Solution Formation and Sintering in the System $BaTiO_3$–$SrTiO_3$, Journal of the American Ceramic Society 65 (1982) 470–474.

[26] E.B. Watson, J.D. Price, Kinetics of the reaction $MgO + Al_2O_3 \rightarrow MgAl_2O_4$ and Al–Mg interdiffusion in spinel at 1200–2000 °C and 1.0–4.0 GPa, Geochimica et Cosmochimica Acta 66 (2002) 2123–2138.

[27] H.R. Zargar, M.R. Bayati, H.R. Rezaie, F. Golestani-Fard, R. Molaei, S. Zanganeh, et al., Influence of nano boehmite on solid state reaction of alumina and magnesia, Journal of Alloys and Compounds 507 (2010) 443–447.

[28] G.K. Layden, M.C. McQuarrie, Effect of minor additions on sintering of MgO, Journal of the American Ceramic Society 42 (1959) 89–92.